BIBECHANA
Vol. 23, No. 3, August 2026, 99–107

ISSN 2091-0762 (Print), 2382-5340 (Online)
Journal homepage: http://nepjol.info/index.php/BIBECHANA
Publisher:Dept. of Phys., Mahendra Morang A. M. Campus (Tribhuvan University)Biratnagar

NuSTAR observations of SWIFT J151857.0-572147 : spectral analysis of the galactic X-ray transient source

Subash Bhandari, Ramesh Neupane, Ramit Dhungana
Shreeram Nagarkoti
St. Xavier's College, Maitighar, Kathmandu, Nepal.

*Corresponding author: Email: cosubhasmos@gmail.com

Abstract

We study the spectral properties of the galactic X-ray transient source SWIFT J151857.0-572147 using two NuSTAR observations from March 2024. The spectral analysis was performed using data from two onboard instruments, FPMA and FPMB of NuSTAR, in the broad energy range of 3–50 *keV. To achieve the best fit, the spectral fitting required a combination of models: constant, power-law, multicolor disk–blackbody continuum, and Gaussian emission/absorption. Results show a hydrogen column density varying from* 2.50 *to* 7.94×10^{22} cm^{-2}. *The inner disk temperature of the source varied from* 0.99 *keV to* 1.04 *keV, and photon indices ranged from* 1.74 *to* 4.08, *indicating a transition from a low/hard to a high/soft state typical of black hole X-ray binaries.*

Keywords
Neutron stars, black hole binaries, X-ray transients, accretion disk, NuSTAR.

Article information
Manuscript received: September 16, 2025; Revised: August 14, 2026; Accepted: August 28, 2026
DOI: https://doi.org/10.3126/bibechana.v23i3.84510

1 Introduction

Black hole X-ray binaries (BHXRBs) are systems that consist of a stellar-mass black hole accreting matter from its companion star. Black hole binaries emit X-rays during their accretion by effectively converting gravitational potential energy into outward radiation. Studying such sources is important to understand the characteristic properties like spin, mass, and accretion properties of the binary system [1]. Intense X-rays are produced during black hole outburst events. These outbursts can occur when the accretion flow from the donor star is not sufficient to support the flow of matter toward the black hole. As a result, the material accumulates in the outer disk until it reaches a critical density. Once this critical surface density is achieved, the disk becomes unstable and rapidly collapses onto the black hole, resulting in a powerful flare of X-ray radiation, including intense X-rays [1–3]. These types of outbursts can recur for several months to several decades [4, 5].

BHXRBs can emit X-rays in different forms, mainly categorized into two major stages based on the type of photon emission. Typical BHXRBs transit from the low/hard state (LHS) when the photon index is comparatively lower to the high/soft state (HSS) when the photon index reaches higher values [1, 6].

Higher photon index are identified by steeper regions in the X-ray spectrum, while softer photon index has a flattened spectrum. A lower photon index indicates the emission of a larger number of photons.

During LHS, the power law component has a smaller value of photon index ($\Gamma < 2$) compared to the soft power law, which means the low photon index has a spectrum with relatively high-energy photons. The thermal component from the accretion disk is either weak or absent in this state [7]. On the other hand, the high/soft state in X-ray binaries can be explained by thermal Comptonization, where low-energy photons gain energy by scattering off the hot electrons in plasma, originating from an optically thick, geometrically thin accretion disk [8]. The transition between the low hard state and the high soft state is called the hard and soft intermediate state, and it typically occurs at an accretion rate of a few percent of the Eddington limit [9]. During this transition, Γ will increase significantly from 1.4–1.8 to approximately 2.5 and above [9, 10]. These states are also often associated with the launching and quenching of relativistic jets [11].

Swift J151857.0-572147 (hereafter *Swift J151857*) is the new Galactic transient which was first detected by *Swift/XRT* as a *GRB 20240303A* [12], in Swift Trigger 1218452 (GCN 35849). However, the repeated observations of the source indicated that it remained persistently bright, with no signs of fading, which confirmed its nature as a Galactic Transient [13]. The Right Ascension (RA) and Declination of the source were found to be RA(J2000) = 15h 18m 57.00s and Dec(J2000) = -57d 21' 47.9" [13]. Later, follow-up observations with the Australia Telescope Compact Array (ATCA) at central frequencies of 5.5 GHz and 9 GHz revealed bright radio flares [14], which are typically obtained for BHXRB transients undergoing transition from hard spectral state to soft spectral state.

Follow-up observation by Del Santo et al. [15] showed that the X-ray spectrum was significantly softer than in the previous XRT observation [12], described by an absorbed disk black-body plus a power-law model with a reduced $\chi^2 = 1.07$ (618 degree of freedom), with the equivalent hydrogen column of $(4.4 \pm 0.3) \times 10^{22}$ cm^{-2}, a photon index of $2.2(-0.4, +0.3)$ and an inner disk temperature of 0.81 ± 0.06 keV. The parameters found by [15] were consistent with those of typical Galactic black hole X-ray binaries in a soft or soft/intermediate state.

Our work focuses on spectral analysis using specific NuSTAR observations to investigate the source's spectral properties, such as the power-law index and disk temperature during its 2024 outburst. We fit the X-ray spectra in a broadband energy range 3–50 keV, using different combinations of models in `XSPEC`. Finally, we obtain best-fit parameters and extract important properties of the source to conclude our work.

The paper is organized as follows: in Section 2, we discuss the observation and data reduction procedure. In Sections 3, we discuss the results of the spectral data analysis, and finally, draw our conclusions in Section 4.

2 Observation and data reduction

Swift J151857 was observed by NuSTAR on March 17 and 18, 2024, with exposures of 13885 s and 9195 s, respectively. The corresponding observation IDs and their details are shown in Table 1. We include NuSTAR observations 91001311002 and 91001311004 in our analysis and write each observation ID as data Group 1–4 for 91001311002A, 91001311002B, 91001311004A, and 91001311004B, respectively. The data were reduced with the HEASOFT V6.34/NuSTAR Data Analysis Software (`NUSTARDAS`) pipeline, version 2.1.4, and `CALDB` version 20241216. The source region was extracted as a circle of 60 arcsec radius, centered at the peak brightness, and a background was determined from a circle of 60 arcsec radius with the lowest apparent source contamination, using `ds9` [16]. We used `XSPEC` [17] version 12.14.1, a visualization software for spectral analysis and further fitting. The χ^2 statistic is used to test the goodness of the fit throughout the analysis.

During the outburst, the NuSTAR observations showed that the source *Swift J151857* stayed in a Low hard state (LHS) before 10th March 2024 and gradually transitioned into the soft state after 10th March 2024 [12, 13, 18]. The Low hard state is characterized by hard X-ray emission produced by Comptonized emission from the corona, and soft X-rays and minimal variability characterize the soft state.

Table 1: NuStar observations of the source Swift J151857 for each instrument FPMA/FPMB during the 2024 outburst

ObsID	Date observed	Exposure(s)	counts
91001311002A	2024-03-17	13880	157.0
91001311002B	2024-03-07	14300	146.8
91001311004A	2024-03-18	9195	140.1
91001311004B	2024-03-07	9449	131.3

3 Results and discussion

The NuSTAR observations contained spectra in the range 3–79 keV, but we restricted the spectra to the 3–50 keV range, as below 3 keV and above 50 keV, the count rate drops steeply to near the background level, accompanied by large statistical uncertainties. The NuSTAR observations of the source with observation ID 91001311002 for both FPMA and FPMB contained 157.0, and 146.8 net counts with exposure time of 13880 s and 14300 s respectively, and that for 91001311004 contained 140.1, and 131.3 net counts with exposure time of 9195 s and 9449 s respectively. We fit each of the FPMA/FPMB observations to the model using the XSPEC spectral fitting package. Our combination includes a couple of multiplicative and additive models. Each of the models was multiplied by `const`, a scaling factor to ensure normalization, and the absorption component `tbabs`. The obtained results and parameters for each model are discussed in the following sections.

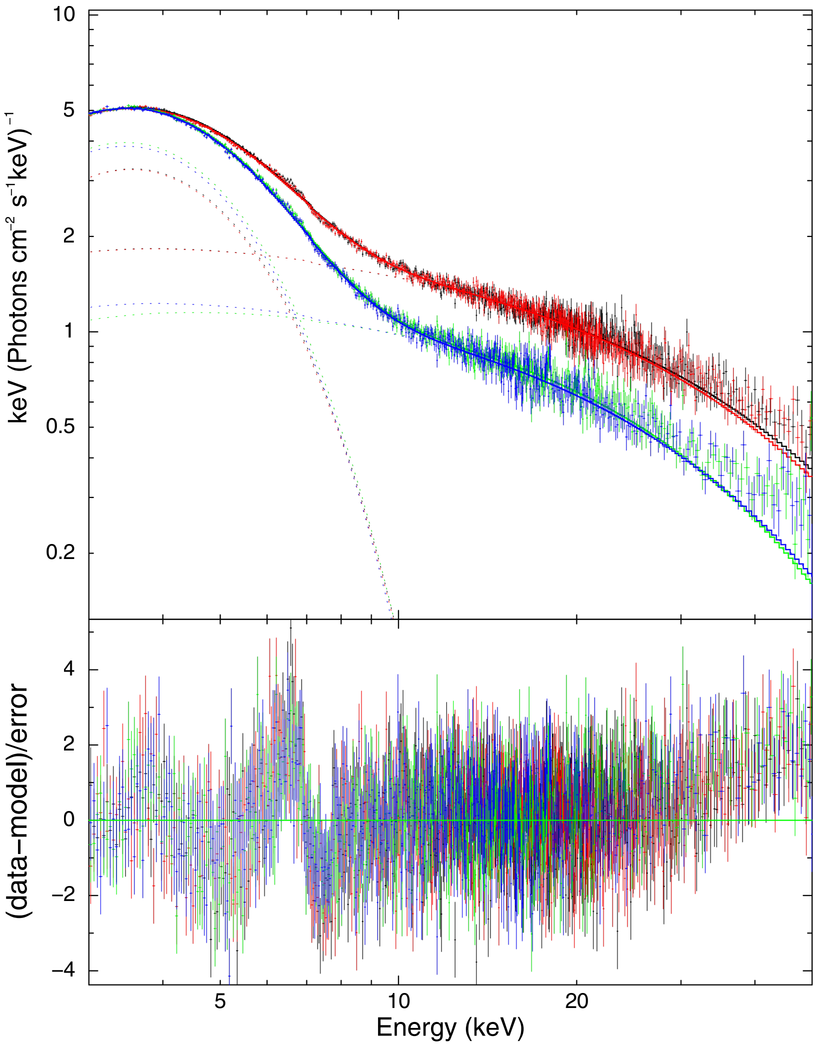

Figure 1: Spectra and models for the fit with `constant*tbabs*(bbody+cutoffpl)` for the source. The black, red, green, and blue lines in the top panel represent each spectrum (FPMA/B) listed from top to bottom in Table 1. The bottom panel shows the residuals in terms of sigmas; the colors are the same as in the top panel.

3.1 bbody + cutoffpl

Initially, we start with the simple model with a single disk blackbody component to model the emission as arising from a single-temperature region. The spectra from all observations were fitted to the single-temperature disk blackbody model `bbody`, added with a super-exponential cutoff absorption model `cutoffpl`. The final model is read as `constant*tbabs(bbody + cutoffpl)` in XSPEC. For this model, the best-fit hydrogen column density was obtained to be higher for all observations than the average value along the line of sight,

$5.31 \times 10^{19}\text{cm}^{-2}$ [19], possibly due to the relatively few low-energy bins in the observations' spectra. The model is also best fit to photon index (Γ) with the value in the range 1.895±0.067 to 2.084±0.042, which is less than 2.6, that which was obtained by Peng et al [20].

Table 2: Best-fit parameters for model `constant *tbabs*(bbody + cutoffpl)` for all observations. Data groups correspond to observation IDs.

Component	Parameter	Unit	Group 1	Group 2	Group 3	Group 4
`tbabs`	N_H	10^{22}	0.968 ± 0.113	0.889 ± 0.115	0.859 ± 0.127	0.949 ± 0.135
`bbody`	kT	keV	0.847 ± 0.004	0.845 ± 0.004	0.827 ± 0.004	0.820 ± 0.005
`cutoffpl`	Γ	—	2.084 ± 0.042	2.057 ± 0.043	1.895 ± 0.067	2.029 ± 0.068
`cutoffpl`	HighECut	keV	31.349 ± 2.147	29.009 ± 1.897	20.001 ± 1.462	23.251 ± 2.007

Reduced χ^2_ν (dof) = 1.153.

In Figure 1, the top panel shows the unfolded spectra of the four FPMA/B observations with colors black, red, green, and blue representing observation IDs listed from top to bottom in Table 1, together with the best-fit model shown by solid lines and its two additive components, a soft `bbody` component and a harder `cutoffpl` component, shown by the dotted lines. The blackbody component appears as a soft excess visually peaking around 1–2 keV and an absorption component dominating at higher energies. The spectral fit parameters presented in Table 2 provide insights into the physical properties of the observed source fitted with this model. The high-energy cutoff (20–31 keV) reflects the coronal temperature, with lower cutoffs in Group 3 suggesting a cooler corona during that observation. The blackbody temperature ($kT \sim 0.82$–0.84 keV) is consistent with a warm accretion disk, but the single-temperature assumption may oversimplify the disk's radial temperature profile. The acceptable χ^2 indicates a good fit, but residuals suggest the need for a more complex thermal component.

3.2 diskbb + cutoffpl

The `bbody` model was insufficient to capture the complexity of the thermal emission in accreting systems, because it was a single-temperature component model and it lacked the property to account for a radial temperature gradient. To address this limitation, we adopted the `diskbb`, a multi-temperature disk blackbody component that accounts for the radial temperature gradient inherent in a geometrically thin, optically thick accretion disk [21]. The `diskbb` model represents the disk as a sum of blackbody spectra emitted from concentric annuli, each with a different temperature decreasing outward from the center. The spectra were reasonably fitted to the multi-temperature disk blackbody model `diskbb`, to account for an accretion disk consisting of multiple blackbody components, added with a super-exponential cutoff absorption model `cutoffpl`, to account for curvature at higher energies. The final model is read as `constant*tbabs(diskbb + cutoffpl)` in XSPEC.

The transition to this enabled a more physically motivated and accurate characterization of the thermal component in our spectral fits, with an improved value of χ^2 (1.101) with 4696 degrees of freedom (dof). Table 3 presents the best-fit parameters derived from fitting a model to observational data across four distinct groups, corresponding to different observation IDs. The best-fit hydrogen column density was obtained to be higher for all observations than the average value along the line of sight, $5.31 \times 10^{19}\text{cm}^{-2}$. This might be possible due to the relatively few low-energy bins in the observations' spectra, which are simply leading to a poor constraint on the column density. The model is also best fit to photon index (Γ) with the value ranging from 1.74 (Group 3) to 4.08 (Group 1). As observed, the value of Γ for Group 1 is significantly higher than that for other observations due to the intrinsic spectral state changes in the source, potentially associated with variations in the accretion disk-corona system. Alternatively, the higher value of photon index may indicate transient changes, such as the onset of a soft excess component or a transition towards a more disk-dominated spectral state [1]. The inner disk temperature (T_{in}) shows an anomalously high value for Group 1 (8.38 keV), which is unphysical and could result from model degeneracy or fitting artifacts. Typical T_{in} values (0.998–1.041 keV) for Groups 2–4 align with BHXRBs in the soft state. The high-energy cutoff range 17.470 keV (Group 3) to 25.629 keV (Group 2) reflects coronal dynamics, with lower cutoffs indicating a cooler corona. However, the value for Group 1, 106.742, is marginally higher, indicating poor constraint of the parameter with the current model.

The spectral fit and residuals are plotted in Figure 2. The top panel shows the unfolded spectra of the four FPMA/B observations with colors black, red, green, and blue representing observation IDs listed from top to bottom in Table 1. The best-fit model is shown by solid lines, and dotted lines represent its two additive components: a soft `diskbb` component and a harder `cutoffpl` component. The spectra show a prominent thermal peak around a few keV, consistent with the `diskbb` component and characteristic of a multi-temperature accretion disk. A high-energy tail extending beyond 10 keV is seen, which is well described by the `cutoffpl` component and typically attributed to Comptonized emission from a hot corona. The bottom panel shows the fit residuals, which are randomly scattered around zero across the full energy range with no systematic structure, indicating that this two-component model provides a statistically acceptable description of the data, with an obtained value of χ^2/dof as 1.101.

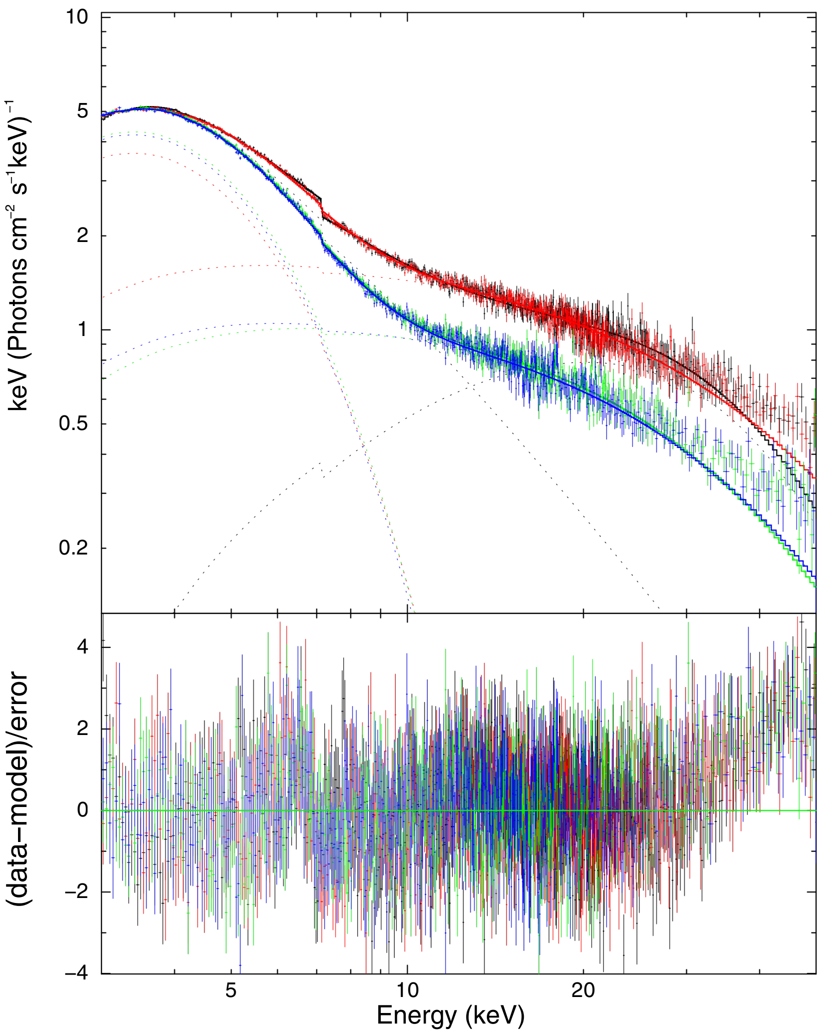

Figure 2: Spectra and models for the fit with `constant*tbabs*(diskbb+cutoffpl)` for the source. The black, red, green, and blue lines in the top panel represent each spectrum (FPMA/B) listed from top to bottom in Table 1. The bottom panel shows the residuals in terms of sigmas; the colors are the same as in the top panel.

Table 3: Best-fit parameters for model `constant*tbabs*(diskbb + cutoffpl)` for all observations. Data groups correspond to observation IDs.

Component	Parameter	Unit	Group 1	Group 2	Group 3	Group 4
tbabs	N_H	10^{22}	7.936 ± 0.162	2.505 ± 0.096	2.836 ± 0.106	2.865 ± 0.112
diskbb	$T_{\rm in}$	keV	8.384 ± 0.082	1.041 ± 0.007	1.008 ± 0.007	0.998 ± 0.007
cutoffpl	Γ	—	4.082 ± 0.092	1.961 ± 0.048	1.743 ± 0.075	1.889 ± 0.076
cutoffpl	HighECut	keV	106.742 ± 182.451	25.629 ± 1.603	17.470 ± 1.212	20.128 ± 1.627

Reduced χ^2_ν (dof) = 1.101.

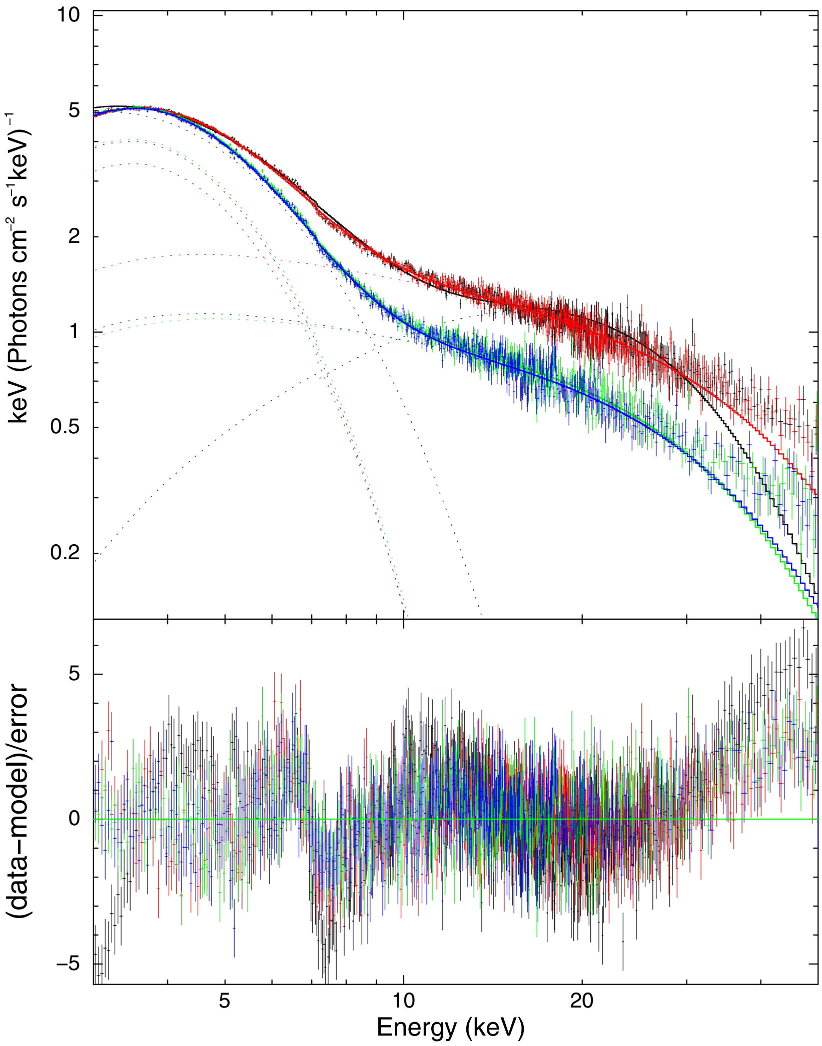

Figure 3: Spectra and models for the fit with `constant*tbabs*(diskbb+nthcomp)` for the source. The black, red, green, and blue lines in the top panel represent each spectrum (FPMA/B) listed from top to bottom in Table 1. The bottom panel shows the residuals in terms of sigmas; the colors are the same as in the top panel.

3.3 diskbb + nthcomp

We tried to check for a Gaussian signature by adding a `gaussian` component in our model `constant*tbabs*(diskbb+cutoffpl)`, which was found insignificant, as there were no significant residuals around 5–7 keV, which suggests that there is no Fe-Kα emission line. To verify the result we obtained, we replaced the `cutoffpl` component with `nthcomp`, a thermally Comptonized continuum model of [22]; as later extended by [23], which offers a sharper high-energy cut-off and a more accurate low-energy rollover with similar parameters. The redshift (z) and seed photon temperature (kT_{bb}) were frozen and fixed to 0.06 and 0.7 keV. The χ^2 was calculated to be 1.384 with 4696 degrees of freedom (dof), a poorer fit than our previous model. The best-fit hydrogen column density (N_H) was obtained to be in the range from 3.09–3.19$\times 10^{22}$cm^{-2}, which is higher for all observations than the average value along the line of sight, 5.31×10^{19}cm^{-2}. However, the value is much less than 4–5 $\times$ 10^{22}cm^{-2}, obtained by Mondal et al. [24]. The photon index (Γ) is poorly constrained compared to other models, with the value in the range from 2.16 to 2.80.

Table 4: Best-fit parameters for model `constant*tbabs*(diskbb + nthcomp)` for all observations. Data groups correspond to observation IDs.

Component	Parameter	Unit	Group 1	Group 2	Group 3	Group 4
tbabs	N_H	10^{22}	3.087 ± 0.125	3.087 ± 0.125	3.176 ± 0.124	3.187 ± 0.128
diskbb	T_{in}	keV	6.698 ± 0.041	1.023 ± 0.007	1.001 ± 0.006	0.992 ± 0.006
nthcomp	Γ	—	2.804 ± 0.026	2.235 ± 0.017	2.165 ± 0.025	2.222 ± 0.026
nthcomp	kT_e	keV	1.624 ± 0.024	11.831 ± 0.477	8.772 ± 0.342	9.622 ± 0.455

Note. Reduced χ^2_ν (dof) = 1.384.

Table 4 presents the best-fit parameters for this model. The N_H values 3.087–3.187$\times 10^{22}$ cm^{-2} are lower than those in the `diskbb+cutoffpl` model but still exceed the Galactic average, suggesting intrinsic absorption. The photon index range 2.16 to 2.80 indicates a softer spectrum than the `cutoffpl` models, consistent with a soft/intermediate state. The inner disk temperature (T_{in}) for Group 1 (6.698 keV) is unusually high, potentially due to fitting issues or model limitations. Other T_{in} values (0.992–1.023 keV) are typical for BHXRBs. The coronal temperature (kT_e) and seed photon temperature (kT_{bb}) in `nthcomp` provide insights into the Comptonization process, but their identical values across observations (e.g., 6.698 keV for Group 1) suggest parameter degeneracy. The higher χ^2 indicates that `nthcomp` is less suitable for this dataset, possibly due to its sharper high-energy cutoff.

Figure 3 shows the fitted model with spectra. The top panel shows the unfolded spectra of the four FPMA/B observations with colors black, red, green, and blue representing observation IDs listed from top to bottom in Table 1. The best-fit model is shown by solid lines, while dotted lines represent its two additive components: `diskbb` and `nthcomp`. The bottom panel shows the fit residuals, which seem to be more distorted than in the previous model, and hence no significant conclusions can be drawn with the addition of the Comptonization model.

4 Conclusion

Our spectral analysis of Swift J151857 using NuSTAR observations during its 2024 outburst further supports its classification as a galactic X-ray transient, likely a BHXRB in the soft or intermediate state. The `constant*tbabs*(diskbb+cutoffpl)` model best fits the 3–50 keV spectra ($\chi^2 = 1.101$, 4696 dof), revealing a multi-temperature accretion disk ($T_{in} \approx 0.99$–1.04 keV) and a Comptonized corona ($\Gamma \approx 1.7$–4.0, high-energy cutoff 17.4–106.7 keV). The high hydrogen column density ($N_H \approx 2.50$–7.94×10^{22}cm^{-2}) suggests intrinsic absorption, while the absence of Fe-Kα emission indicates minimal reflection.

The source's high luminosity (6.10–7.30 $\times$ 10^{46}erg s^{-1}) and spectral softening align with a high accretion rate, potentially near the Eddington limit. Comparisons with Del Santo et al. [15] and Peng et al. [20] show consistency in disk temperature and photon index, reinforcing the BHXRBs' interpretation. However, discrepancies in N_H and the anomalous T_{in} for Group 1 highlight the need for further soft X-ray and multi-wavelength data. Further analysis with joint observations can be done to remove the discrepancy and constrain more insightful conclusions from the model.

Acknowledgments

This research has made use of the NuSTAR Data Analysis Software (NuSTARDAS) jointly developed by the ASI Space Science Data Center (SSDC, Italy) and the California Institute of Technology (Caltech, USA). We acknowledge the use of XSPEC (version 12.14.1) for spectral analysis and SAOImage DS9 for data visualization. We are grateful to our colleagues for their valuable discussions and feedback that improved this work.

Authors' contributions

SB: Writing, Methodology, Formal analysis. RN: Software, Visualization. RD: Analysis, Editing. SN: Resources, Validation, Supervision, Review & Editing.

Declarations and conflict of interest

There is no conflict of interest by the authors.

References

[1] Remillard RA, McClintock JE. X-Ray Properties of Black-Hole Binaries [Journal Article]. Annual Review of Astronomy and Astrophysics. 2006;44:49-92. Available from: https://www.annualreviews.org/content/journals/10.1146/annurev.astro.44.051905.092532.

[2] Lasota JP. The disc instability model of dwarf novae and low-mass X-ray binary transients. New Astronomy Reviews. 2001 Jun;45(7):449-508.

[3] Dubus G, Hameury JM, Lasota JP. The disc instability model for X-ray transients: Evidence for truncation and irradiation. Astronomy & Astrophysics. 2001 Jul;373:251-71.

[4] Tanaka Y. In: Bleeker JAM, Geiss J, Huber MCE, editors. Black-hole binaries. Dordrecht: Springer Netherlands; 2001. p. 839-56. Available from: https://doi.org/10.1007/978-94-010-0320-9_36.

[5] Chen W, Shrader CR, Livio M. The Properties of X-Ray and Optical Light Curves of X-Ray Novae. The Astrophysical Journal. 1997 Dec;491(1):312-38.

[6] Belloni T, Homan J, Casella P, van der Klis M, Nespoli E, Lewin WHG, et al. The evolution of the timing properties of the black-hole transient GX 339–4 during its 2002/2003 outburst. Astronomy & Astrophysics. 2005 August;440(1):207-22. Available from: http://dx.doi.org/10.1051/0004-6361:20042457.

[7] Esin AA, McClintock JE, Narayan R. Advection-Dominated Accretion and the Spectral States of Black Hole X-Ray Binaries: Application to Nova Muscae 1991. The Astrophysical Journal. 1997 November;489(2):865-89.

[8] Shakura NI, Sunyaev RA. Black holes in binary systems. Observational appearance. Astronomy & Astrophysics. 1973 January;24:337-55.

[9] Maccarone TJ, Coppi PS. Hysteresis in the light curves of soft X-ray transients. Monthly Notices of the Royal Astronomical Society. 2003 Jan;338(1):189-96.

[10] Gierlinski M, Newton J. X-ray spectral transitions of black holes from RXTE All-Sky Monitor. Monthly Notices of the Royal Astronomical Society. 2006 Aug;370(2):837-44. Available from: http://dx.doi.org/10.1111/j.1365-2966.2006.10514.x.

[11] Fender RP, Belloni TM, Gallo E. Towards a unified model for black hole X-ray binary jets. Monthly Notices of the Royal Astronomical Society. 2004 December;355(4):1105-18.

[12] Kennea JA, Lien AY, D'Elia V, Melandri A, Page KL, Siegel MH. Swift J151857.0-572147: Swift detection of a new galactic X-ray transient. The Astronomer's Telegram. 2024 March;16500:1.

[13] Kennea JA, Lien AY, Page KL, Neil Gehrels Swift Observatory Team. Swift J151857.0-572147: Confirmation of a new galactic transient. GRB Coordinates Network. 2024 March;35853:1.

[14] Carotenuto F, Russell TD. ATCA detection of an extremely bright radio flare from Swift J151857.0-572147. The Astronomer's Telegram. 2024 Mar;16518:1.

[15] Del Santo M, Russell TD, Marino A, Motta S. Swift/XRT observation of Swift J151857.0-572147 indicates that the source likely made a transition to the soft state. The Astronomer's Telegram. 2024 March;16519:1.

[16] Joye WA, Mandel E. New Features of SAOImage DS9. In: Payne HE, Jedrzejewski RI, Hook RN, editors. Astronomical Data Analysis Software and Systems XII. vol. 295 of Astronomical Society of the Pacific Conference Series; 2003. p. 489.

[17] Arnaud KA. XSPEC: The First Ten Years. In: Jacoby GH, Barnes J, editors. Astronomical Data Analysis Software and Systems V. vol. 101 of Astronomical Society of the Pacific Conference Series; 1996. p. 17.

[18] Del Santo M, Russell TD, Marino A, Motta S. Swift/XRT observation of Swift J151857.0-572147 indicates that the source likely made a transition to the soft state. The Astronomer's Telegram. 2024 March;16519:1.

[19] HI4PI Collaboration, Ben Bekhti, N , Flöer, L , Keller, R , Kerp, J , Lenz, D , et al. HI4PI: a

full-sky H I survey based on EBHIS and GASS. Astronomy & Astrophysics. 2016;594:A116. Available from: https://doi.org/10.1051/0004-6361/201629178.

[20] Peng JQ, Zhang S, Shui QC, Chen YP, Zhang SN, Kong LD, et al. Insight-HXMT, NICER, and NuSTAR Views to the Newly Discovered Black Hole X-Ray Binary Swift J151857.0–572147. The Astrophysical Journal Letters. 2024 Sep;973(1):L7. Available from: http://dx.doi.org/10.3847/2041-8213/ad74ec.

[21] Mitsuda K, Inoue H, Koyama K, Makishima K, Matsuoka M, Ogawara Y, et al. Energy spectra of low-mass binary X-ray sources observed from Tenma. Publications of the Astronomical Society of Japan. 1984 Jan;36:741-59.

[22] Zdziarski AA, Johnson WN, Magdziarz P. Broad-band γ-ray and X-ray spectra of NGC 4151 and their implications for physical processes and geometry. Monthly Notices of the Royal Astronomical Society. 1996 Nov;283(1):193-206.

[23] Życki PT, Done C, Smith DA. The 1989 May outburst of the soft X-ray transient GS 2023+338 (V404 Cyg). Monthly Notices of the Royal Astronomical Society. 1999 Nov;309(3):561-75.

[24] Mondal S, Suribhatla SP, Chatterjee K, Singh CB, Chatterjee R. The first detection of X-ray polarization in a newly discovered Galactic transient Swift J151857.0-572147; 2024. Available from: https://arxiv.org/abs/2404.09643.